RESEARCH ARTICLE

Distinct bacterial assemblages reside at different depths in Arctic multiyear sea ice

Ido Hatam[1], Rhianna Charchuk[1], Benjamin Lange[2,3], Justin Beckers[3], Christian Haas[3] & Brian Lanoil[1]

[1]Department of Biological Sciences, University of Alberta, Edmonton, AB, Canada; [2]Alfred Wegener Institute, Helmholtz Centre for Polar and Marine Research, Bremerhaven, Germany; and [3]Department of Earth and Atmospheric Sciences, University of Alberta, Edmonton, AB, Canada

Correspondence: Brian Lanoil, Department of Biological Sciences, University of Alberta, Edmonton, AB, Canada T6G2E9.
Tel.: +1 780 248 1452;
fax: +1 780 492 9234;
e-mail: brian.lanoil@ualberta.ca

Present address: Christian Haas, Department of Earth & Space Sciences & Engineering, York University, Toronto, ON, Canada M3J1P3

Received 7 May 2014; revised 25 June 2014; accepted 30 June 2014. Final version published online 29 July 2014.

DOI: 10.1111/1574-6941.12377

Editor: Max Häggblom

Keywords
sea ice; depth profile; bacteria.

Abstract

Bacterial communities in Arctic sea ice play an important role in the regulation of nutrient and energy dynamics in the Arctic Ocean. Sea ice has vertical gradients in temperature, brine salinity and volume, and light and UV levels. Multiyear ice (MYI) has at least two distinct ice layers: old fresh ice with limited permeability, and new saline ice, and may also include a surface melt pond layer. Here, we determine whether bacterial communities (1) differ with ice depth due to strong physical and chemical gradients, (2) are relatively homogenous within a layer, but differ between layers, or (3) do not vary with ice depth. Cores of MYI off northern Ellesmere Island, NU, Canada, were subsectioned in 30-cm intervals, and the bacterial assemblage structure was characterized using 16S rRNA gene pyrotag sequencing. Assemblages clustered into three distinct groups: top (0–30 cm); middle (30–150 cm); and bottom (150–236 cm). These layers correspond to the occurrence of refrozen melt pond ice, at least 2-year-old ice, and newly grown first-year ice at the bottom of the ice sheet, respectively. Thus, MYI houses multiple distinct bacterial assemblages, and *in situ* conditions appear to play a less important role in structuring microbial assemblages than the age or conditions of the ice at the time of formation.

Introduction

Sea ice is a habitat for a diverse and active microbial community (Junge *et al.*, 2004, 2006; Mock & Thomas, 2005). The most easily recognizable feature of this community is an algal bloom, usually dominated by diatoms, covering the bottom 10 cm of the ice sheet during the spring and summer (Gosselin *et al.*, 1997; McMinn & Hegseth, 2007; McMinn *et al.*, 2007). Heterotrophic bacteria are key regulators of this bloom and of the subsequent energy and organic matter flux from the ice to underlying seawater via the microbial loop (Poltermann, 2001; Deming, 2007). Furthermore, during the polar winter, heterotrophic production and growth fertilizes the ice in preparation for the spring and summer bloom (Riedel *et al.*, 2008) and supplies the ice and underlying water column with a small but stable subsidy of organic matter through secondary production (Wing *et al.*, 2012).

Microorganisms that colonize sea ice are exposed to a wide array of *in situ* conditions. As the sea ice forms, salts within the water are excluded from the ice crystals, forming a porous matrix of ice and saline brine, with brine salinity and brine volume negatively and positively correlated with the temperature of the surrounding ice, respectively. These brines are interconnected within the ice; thus, sea ice could be considered a semi-solid brine matrix. Channels and pockets of brine within the matrix are permeable (and thus can exchange brine) at a brine volume of *c.* 5% which normally occurs when the temperature is *c.* −5 °C for a typical bulk salinity of the ice of *c.* 5‰ (Golden *et al.*, 1998). Winter and early spring sea ice has a strong temperature gradient, with the top surface of the ice or snow exposed to temperatures as cold as −40 °C and the bottom of the ice at a constant −1.86 °C (Eicken, 2008). Thus, brines near the top of the ice are as much as fivefold more saline and are more isolated from each other than those near the ice-water

FEMS MICROBIOLOGY ECOLOGY

interface, leading to extreme conditions for the microorganisms in the upper sea ice layers (Collins *et al.*, 2010). Furthermore, as a consequence of this temperature gradient, brine volume increases with depth (Wadhams, 2000), and both light intensity and ultraviolet radiation intensity decrease with ice depth due to scattering of incident light by the ice. Higher intensity of UV irradiation at the upper portions of the ice leads to higher oxidative stress than in deeper samples (King *et al.*, 2005). The vast majority of microorganisms within the ice reside within the brine matrix (Junge *et al.*, 2001); thus, sea ice microorganisms experience less extreme environmental conditions, with higher temperatures, lower salinity, increased brine volume, lower UV irradiation, and lower oxygen radical concentration, with increasing depth.

Sea ice is also a highly dynamic environment: the extent of sea ice in the Arctic region fluctuates by more than twofold between minimal and maximal coverage in summer and winter, respectively (Comiso, 2010). Thus, some Arctic sea ice is perennial, that is, ice that has persisted through more than one summer (known as multiyear ice, or MYI), while other ice is seasonal (known as first-year ice, or FYI). MYI proportions in the Arctic have dwindled rapidly over the past few decades (from > 70% of total Arctic sea ice *c.* 1980 to *c.* 45% today), and the Arctic Ocean is expected to be MYI-free by end of the century (Boé *et al.*, 2009; Maslanik *et al.*, 2011). The implications of these shifts to Arctic Ocean ecosystem dynamics are not well understood.

In spring, MYI consists of at least two layers: an old layer that survived the previous season's melt, and a new layer that is added to the bottom of the ice during the seasonal freeze period. The old ice layer undergoes a process of desalination due to gravitational brine drainage and fresh water flushing from snowmelt (Wadhams, 2000; Eicken, 2008). This flushing, along with the growth of new ice, leads to strong vertical stratification in the bulk concentrations (as opposed to brine concentrations) of solutes and particulate organic matter in MYI (Wadhams, 2000; Eicken, 2008). The old ice layer has lower bulk brine volumes than the new ice layer and is less permeable (Eicken, 2008). Melt water also tends to accumulate at low points on the uneven surface of MYI, creating fresh water melt ponds that become incorporated into the sea ice upon freezing (Wadhams, 2000; Jungblut *et al.*, 2009), potentially acting as a source of microbial inoculum into the sea ice (Harding *et al.*, 2011). In these areas, the upper 15–30 cm of ice is comprised of fresh water (Wadhams, 2000), thereby adding another layer of complexity to the ice structure.

Despite these differences in the ice with depth, previous studies of Arctic sea ice bacterial assemblages were of vertically homogenized ice cores. In this study, we characterized the bacterial assemblage composition of different depths of a MYI core from the Lincoln Sea to determine whether the physical and chemical stratification in MYI leads to niche differentiation within the ice. We explore whether bacterial communities (1) differ with ice depth due to strong physical and chemical gradients, (2) are relatively homogenous within a layer, but differ between layers, or (3) do not vary with ice depth.

Materials and methods

Site description and sample collection

In collaboration with the Canadian Arctic Sea Ice Mass Balance Observatory (CASIMBO https://sites.google.com/a/ualberta.ca/casimbo/) expedition during May 2011, two sea ice cores and underlying water samples (SW1, SW2) were sampled at one site on landfast ice off the northern shore of northern Ellesmere Island Nunavut, Canada (82.54905°N, −62.37685°W). The landfast ice had formed from multiyear ice floes which became immobile and embedded in fast ice near the shore during the preceding fall. The site was located in a depression in the ice, implying that a freshwater melt pond was present in summer and that the uppermost ice is, therefore, likely refrozen water from a freshwater pond. This was confirmed by thick section analysis of the ice core texture. An accurate age of the sampled site was not determined; however, the ice was 2.36 m thick, which is typical of MYI and thicker than most FYI. Furthermore, the bulk salinity profile showed an increase in salinity with depth (Fig. 1a), and texture analysis showed the occurrence of a possible annual growth mark at *c.* 125 cm from the surface (Fig. 1b). Therefore, we conclude that the ice appears to have survived at least one melt season.

Two parallel cores were sampled using Kovacs Mark II 9 cm corer (Kovacs Enterprise, Roseburg, Oregon) and a 36 V electric hand drill. Prior to drilling, the core barrel was rinsed with sterile deionized water (Milli-Q Integral Water Purification System, EMD Millipore Corporation, Billerica, MA). The two cores used for 16S rRNA gene pyrotag analysis were immediately sectioned on site to 30-cm intervals using a hand saw (rinsed in deionized water and wiped with an ethanol wipe) and placed in UV-sterilized polypropylene bags. The third core was used for texture analysis and was placed in polypropylene bags with no processing in the field. For seawater sampling, duplicate 2 L samples of water were pumped into polypropylene bags from the coring hole using a manual peristaltic pump (Cole Palmer, Montreal, QC, Canada). Both water and ice samples were covered, kept chilled, and processed within 4 h of sampling. The temperature profile was estimated by measuring the temperature at

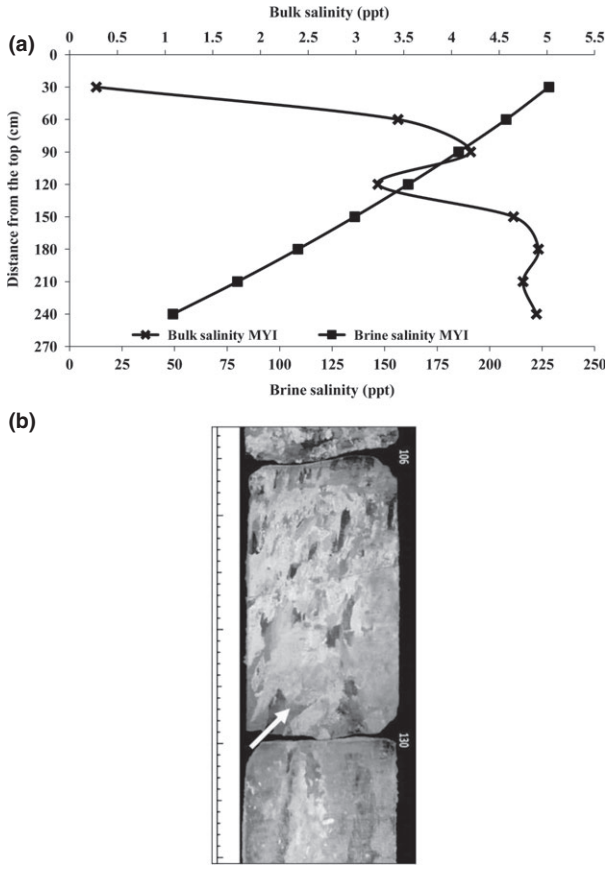

Fig. 1. Chemical and physical attributes of the ice cores. (a) Measured bulk and calculated brine salinity, (b) Texture of ice crystals. The arrow indicates the start of a new layer of columnar ice, marking the annual growth line between 125 and 130 cm depth. Scale bar in cm.

the snow–ice interface and assuming a linear temperature gradient to the ice–water interface (which is at the freezing point of the water, i.e. −1.86 °C) (Supporting Information, Fig. 1a).

Sample processing

Ice samples used for pyrotag analysis were thawed at room temperature in the dark. For each ice section and seawater sample, salinity was measured with an ExStikII® salinity meter (Extech Instruments, Nashua, NH). A portion (45 mL) of each sample was preserved in formaldehyde (3.7% v/v final concentration; Fisher Scientific, Ottawa, ON, Canada) for later cell counts. The remaining ice melt and seawater samples were filtered individually through 0.22-μm-pore-size polyethersulfone membrane filters (Pall, Mississauga, ON, Canada). Direct melting was used to avoid nonspecific addition of DNA and dilution of samples. Although previous studies reported some bacterial cell loss when using direct melting, it has been shown to be appropriate for sea ice bacterial samples (Helmke & Weyland, 1995; Kaartokallio *et al.*, 2005, 2008; Deming, 2010; Ewert *et al.*, 2013). All glassware was sterilized using 10% household bleach solution followed by thorough washing in sterile deionized water between samples to prevent cross-contamination. Each filter was placed in a microfuge tube and submerged in RNA*later*® solution (Life Technologies, Burlington, ON, Canada) and stored at −20 °C for later DNA extraction.

The ice texture core was kept at −10 °C and sectioned to 10-cm intervals using a band saw. Each subsection was then vertically trimmed with a band saw so that only a thin slab 3–5 mm thick from the middle of the core was kept to provide a clean surface for imaging. Each vertical 10-cm core section was exposed to cross-polarized light and photographed using a Panasonic DMC-TZ3 for crystal structure analysis. Cell counts were performed on formaldehyde-fixed, DAPI (Sigma-Aldrich) stained cells with a Leica Microsystems DMRXA epifluorescent microscope (Leica, Concord, ON, Canada) as previously described (Hobbie *et al.* 1977; Porter and Feig 1980).

DNA extraction, amplification, and sequencing

DNA was extracted from preserved filters by bead beating using the FastDNA® SPIN Kit for Soil (MP Biomedicals, Solon, OH) as instructed by the manufacturer. Filters from equivalent 30-cm sections of duplicate ice cores were combined prior to DNA extraction to ensure sufficient DNA yield. Seawater duplicate samples were processed individually.

Molecular Research LP (Shallowater, TX) performed pyrosequencing of the V1-V3 regions of the bacterial 16S rRNA gene as previously described (Dowd *et al.*, 2008). Amplification was performed using HotStarTaq Plus Master Mix Kit (Qiagen, Valencia, CA) under the following conditions: 94 °C for 3 min, followed by 28 cycles of 94 °C for 30 s; 53 °C for 40 s; and 72 °C for 1 min with a final elongation step at 72 °C for 5 min. Gene-specific forward PCR primer sequences were tagged with the sequencing adapters for GS FLX Titanium chemistry, an 8 base barcode, and a linker sequence. All PCRs were performed in triplicate, mixed in equal concentrations, and purified using Agencourt AMPure beads (Agencourt Bioscience Corporation, MA). FLX-Titanium amplicon pyrosequencing was performed using the Genome Sequencer FLX System (Roche, Branford, CT). A list of all primers and barcodes is provided in Supporting Information Table S1.

Preprocessing and quality control of raw sequences

All preprocessing and sequence quality control steps were performed using Mothur v. 1.33.3 following the Mothur 454 SOP (http://www.mothur.org/wiki/454_SOP) (Schloss *et al.*, 2009, 2011). In brief, row flowgram data were used to discard sequences not in the range of 360–720 flows, as recommended (Quince *et al.*, 2011). Noise reduction was performed using the Mothur implementation of the PyroNoise algorithm, which corrects PCR- and pyrosequencing-generated errors using the shhh.flows command, which corrects PCR- and pyrosequencing-generated errors (Quince *et al.*, 2009; Schloss *et al.*, 2011). Sequences shorter than 200 bp or those containing primer/barcode mismatches or homopolymers longer than 8 bp were discarded. Remaining sequences were aligned against the SILVA reference data set and then preclustered for further noise reduction as recommended (Pruesse *et al.*, 2007; Huse *et al.*, 2010; Schloss, 2010; Schloss *et al.*, 2011). Chimeras were detected and removed using the Mothur implementation of UCHIME (Edgar *et al.*, 2011; Schloss *et al.*, 2011). OTUs were assigned using the average-neighbor clustering algorithm for an OTU definition of 97% similarity. The assigned OTUs were classified to phylum, class, and/or genus level using the Ribosomal Database Project classifier (train set 9) with a 60% confidence threshold (RDP; http://rdp.cme.msu.edu/). Based on this classification, sequences of mitochondrial origin were removed from the data set. The sequences were subsampled to the smallest library size ($n = 1800$) to allow identical sequencing depth for each sample before further alpha and beta diversity analyses (Gihring *et al.*, 2012). Sequences were submitted to the National Center for Biotechnology Information Sequence Read Archive under accession number SAMN02768838–SAMN02768847.

Assemblage analysis

Mothur v. 1.33.3 was used for all assemblage analysis and statistics (Schloss *et al.*, 2009). Alpha diversity was estimated using the Chao1 and ACE nonparametric richness estimators, reciprocal Simpson's diversity index (invsimpson), and Shannon diversity index (Shannon, 1948; Simpson, 1949; Chao, 1984; Chao & Shen, 2003). Yue & Clayton's theta measure of dissimilarity (θyc) was used to compare the assemblage structure of all samples in an OTU-based, phylogeny-independent manner (Yue & Clayton, 2005). A UPGMA dendrogram was generated based on the distance matrix resulting from the θyc analysis. The statistical support for clusters in the dendrogram was tested with a Mothur-modified implementation of weighted UniFrac (Lozupone *et al.*, 2006; Schloss *et al.*, 2009). Phylogeny-based analysis of assemblage similarity was performed using the Mothur implementation of unweighted UniFrac (Lozupone *et al.*, 2006; Schloss *et al.*, 2009). For generation of Unifrac scores, a phylogenetic tree was generated with the Mothur implementation of Clearcut using the relaxed neighbor-joining algorithm (Evans *et al.*, 2006; Schloss *et al.*, 2011).

Results

Environmental

The core length (236 cm) and bulk salinity profile (ranging from 0.28 ppt for the top 30 cm to 4.89 ppt for the bottom 30 cm) (Fig. 1a) were typical of MYI (Eicken *et al.*, 1995; Haas, 2004). Based on ice crystal texture analysis, the core had a possible annual growth mark at *c.* 125 cm from the surface of the ice (Fig. 1b), indicating the presence of at least two annual layers. Furthermore, bulk salinity for the topmost layer was extremely low (Fig. 1a), indicating the presence of a former melt pond. Although neither approach is definitive in dating the core, the ice appears to have at least three layers: melt pond (0–30 cm), 2-year-old ice (subsequently referred to as old ice, represented by ice sections from 30 to 150 cm), and first-year ice (subsequently referred to as new ice, represented by ice sections from 150 to 236 cm).

There were strong gradients of temperature and salinity within the ice. The average estimated temperature for the 30-cm intervals ranged from −16.08 °C at the top to −2.81 °C for the bottom (Fig. S1a). Brine salinity, as calculated by the method of Cox & Weeks (1983), ranged from 228.21 ppt at the top to 49.2 ppt at the bottom, reversing the trend observed for the bulk salinity (as expected because the brine salinity is determined solely by temperature) (Fig. 1a). Based on these salinity and temperature profiles, the ice core was permeable to the underlying seawater for only the bottom 90 cm (Golden *et al.*, 1998). Seawater samples had salinities typical of the Arctic Ocean surface waters (Wadhams, 2000): 31.01 ppt and 32.25 ppt for SW1 and SW2, respectively.

Cell counts ranged from high 10^4 to 10^5 cells mL^{-1} of ice melt: these values are on the low end of expected values for sea ice bacterial cell concentration (Junge *et al.*, 2002) (Fig. S1b). A peak in cell concentration was observed at 90 cm depth, which corresponds with a local bulk salinity maximum (Fig. 1a). However, there was no corresponding increase in cell abundance that correlates with the overall bulk salinity maximum at 180 cm depth; thus, it is unclear what *in situ* parameters drive this trend.

The microbial assemblage of the top, middle, and bottom of the ice correspond to the occurrence of three layers of ice, melt pond, old ice, and new ice

The microbial assemblages grouped into three statistically significant ($P < 0.001$) clusters: top (0–30 cm), middle (30–150 cm), and bottom (150–236 cm) (Fig. 2, left panel). These sections match the melt pond, old ice, and new ice sections predicted by ice texture and salinity analysis. Within each group, there appears to be clustering of samples by depth (Fig. 2); however, these clusters were not statistically significant. This apparent clustering indicates that there may be preliminary adaptations to local conditions; however, the ice origin exerts a stronger influence on the microbial assemblage composition.

A phylogeny-based comparison of the assemblages (Lozupone *et al.*, 2006) largely agreed with the OTU-based approach (Table 1). The phylogeny-based comparison, however, indicates that the section from 150 to 180 cm is not significantly different from either the 120 to 150 cm sections or the 180 to 210 cm section and thus 'bridges' the difference between the old ice and new ice sections (Table 1). SW1 and SW2 formed a unique group which excluded all ice samples, supporting the notion that the ice assemblage is distinct from the water assemblage despite the predicted permeability of the bottom 90 cm of ice to seawater (Fig. 2).

Three layers, three assemblage compositions: in-depth look at membership

The melt pond assemblage was dominated by *Bacteroidetes*, which accounted for more than 50% of all sequences. Within this phylum, 90% of the sequences belonged to the class *Flavobacteria*, and *c.* 10% belonged to *Sphingobacteriia* (Fig. 2). Members of the phylum *Actinobacteria* and *Betaproteobacteria* were the second and third most abundant groups, with 27% and *c.* 15% of all sequences, respectively (Fig. 2).

In contrast, the assemblage of the old ice layer included a high abundance of *Alphaproteobacteria,* mainly from the family *Rhodobacteraceae* (ranging from *c.* 20% to 35% of sequences, Fig. 2). Several other groups were also more abundant in this layer when compared to the melt pond, including *Gammaproteobacteria* (*c.* 5–15% of total sequences) and *Sphingobacteria* (*c.* 15% of total sequences). *Verrucomicrobia*, mainly of the class *Opitutae* (*c.* 3% of total sequences), were found in the old ice layer, but were absent from the melt pond ice. Members of the phylum *Actinobac-*

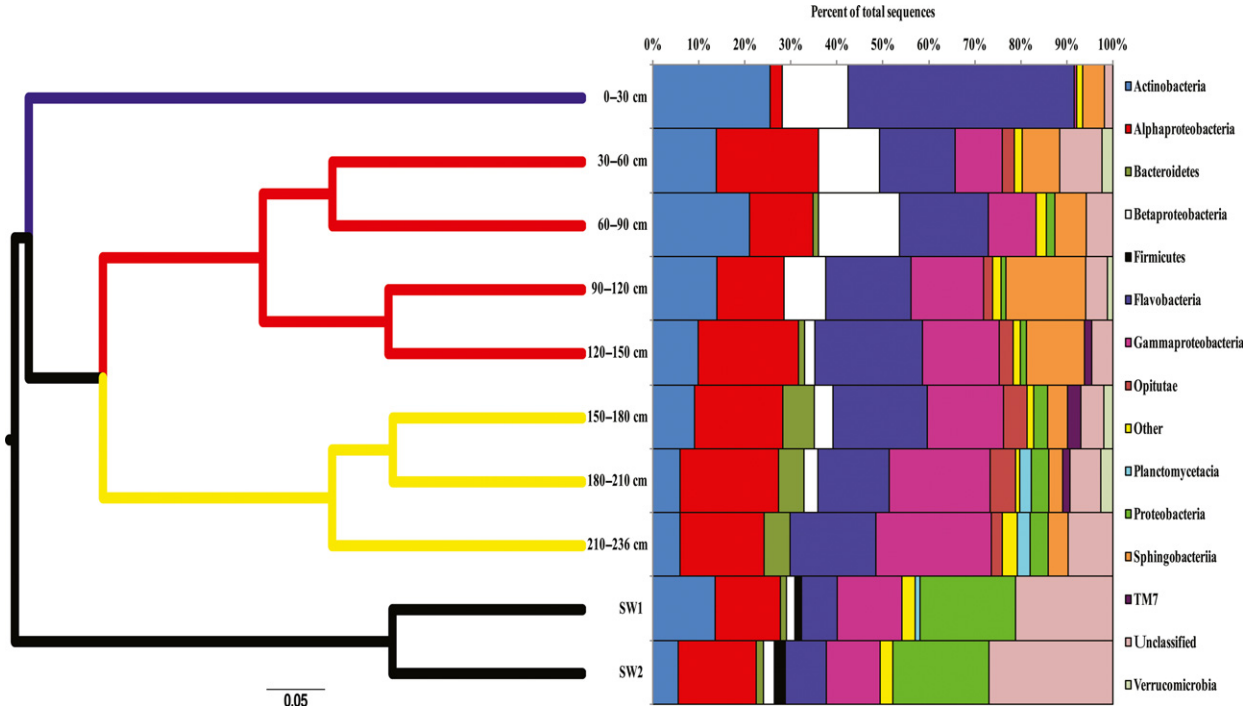

Fig. 2. Similarity and composition of different ice core sections. Samples that are not significantly different ($P < 0.001$) based on weighted Unifrac scores have the same color lines in the clusters. Assemblage composition at the class level is shown for each 30-cm section. Proportion is represented as percent of total sequences per section. Classes that amounted to < 1% of the total sequences per section were pooled as 'other'.

Table 1. Unweighted UniFrac scores for all pairwise comparisons of samples. Samples that are significantly dissimilar ($P \leq 0.001$) are highlighted in grey

	0–30 cm	30–60 cm	60–90 cm	90–120 cm	120–150 cm	150–180 cm	180–210 cm	210–236 cm	SW1	SW2
0–30 cm		0.832	0.823	0.85	0.881	0.906	0.942	0.952	0.958	0.916
30–60 cm	0.832		0.602	0.654	0.712	0.764	0.835	0.867	0.912	0.898
30–90 cm	0.832	0.602		0.616	0.674	0.740	0.827	0.857	0.902	0.894
90–120 cm	0.85	0.654	0.616		0.665	0.721	0.798	0.862	0.896	0.9
120–150 cm	0.881	0.712	0.674	0.665		0.668	0.758	0.831	0.893	0.879
150–180 cm	0.906	0.764	0.740	0.721	0.668		0.693	0.77	0.856	0.848
180–210 cm	0.942	0.835	0.827	0.798	0.758	0.693		0.707	0.859	0.89
210–236 cm	0.952	0.867	0.857	0.862	0.831	0.77	0.707		0.87	0.898
SW1	0.958	0.912	0.902	0.896	0.893	0.856	0.859	0.87		0.757
SW2	0.916	0.898	0.894	0.9	0.879	0.848	0.89	0.898	0.757	

teria (*c.* 10% of sequences) and the class *Flavobacteria* (*c.* 20% of sequences) were lower in this layer, whereas members of the class *Betaproteobacteria* were similar in abundance between the two layers (Fig. 2). Members of the candidate division TM7, while present at low levels throughout the old ice, exceeded 1% of sequences only in the bottom section of the old ice (Fig. 2).

Similar to the old ice assemblage, the new ice assemblage was predominantly comprised of *Alphaproteobactera* mainly from the family *Rhodobacteraceae* (*c.* 30–35% of all sequences, Fig. 2), *Flavobacteria* (*c.* 15% of sequences), and *Gammaproteobacteria* (*c.* 15–25% of sequences). *Verrucomicrobia* of the class *Opitutae* (about 3% of sequences) and members of the candidate division TM7 (*c.* 1–2% of sequences) were more abundant in the bottom layer of ice than the layers above. *Sphingobacteriia* (*c.* 1% of sequences), *Betaproteobacteria* (ranging from 3% to < 1% of sequences), and *Actinobacteria* (ranging from *c.* 6% to 2% of sequences) had lower representation in the new ice assemblage than in the melt pond and old ice assemblages (Fig. 2).

At finer phylogenetic scales, the layers differ further (Table S2, Fig. S3). OTUs belonging to dominant phylogenetic groups differ between the three layers, for example, Flavobacteria from the melt pond assemblage were comprised of sequences belonging almost exclusively (> 98% of sequences classified as *Flavobacteria*) to OTU #1, classified to the genus level as *Flavobacterium*. While this OTU was a dominant member of *Flavobacteria* in the old ice assemblage (*c.* 25% of sequences classified as *Flavobacteria*), there were other OTUs associated with the *Flavobacteria* order and sequences closely related to *Ulvibacter* (*c.* 20% of the sequences classified as *Flavobacteria*, OTU #7), and the genus *Polaribacter* (*c.* 20% of the sequences classified as *Flavobacteria,* OTU #17) were abundant. Furthermore, OTU #1 was absent from the new ice assemblage; which was dominated by OTUs #7 (30% of the sequences classified as *Flavobacteria*) and #17 (15% of the sequences classified as *Flavobacteria*), along with sequences closely related to the genus *Maribacter* (30% of the sequences classified as *Flavobacteria*, OTU #16), sequences closely related to the genus *Winogradskyella* and an unclassified *Flavobacteria* (10% of the sequences classified as *Flavobacteria* each OTU #21 & #23, respectively). OTU# 23 also appeared in the seawater samples (data not shown) and classified by NCBI BLAST as related to the genera *Flexibacter, Flexithrix, and Microscilla* (91% similarity).. All dominant phylum-level groups showed similar variability in the OTU-level composition between layers, even where phylum-level groups were similar (Table S2, Fig. S3).

The seawater microbial assemblage was distinct from the sea ice microbial assemblage (Fig. 2). SW1 and SW2 were *c.* 98% similar to each other. Both were dominated by bacteria unclassified at the phylum level, which represented *c.* 20% and 25% of the total sequences, respectively. Of the classifiable sequences, *Proteobacteria*, with *Alphaproteobacteria* as the major class, dominated seawater (*c.* 20% of the sequences). However, unlike in the sea ice assemblages, where *Rhodobacteracaea* were the dominant *Alphaproteobacteria*, the majority of the seawater *Alphaproteobacteria* sequences belonged to the *Pelagibacteraceae* family (data not shown). Unlike in the ice samples, *Bacteroidetes* in seawater were only represented by *Flavobacteria* (*c.* 5% of the sequences) and unclassified groups (*c.* 3% of the sequences). TM7, *Opitutae*, and other *Verrucomicrobia* were absent from water samples. *Firmicutes* were identified in the water samples (*c.* 5% of sequences), but not in the ice (Fig. 2).

Although Good's coverage estimate shows that sequence coverage was high, with the lowest coverage at 84% (bottom 30 cm of the ice, data not shown), both rarefaction analysis and the ratio of observed OTU to the number of OTU predicted by the Chao1 estimator show that the samples were not sequenced to saturation (Fig. 2a). Thus, these analyses of microbial assemblage should be viewed with some caution as relative abundances might shift with increased taxon coverage.

Taxon richness and overall diversity vary with ice source

The observed OTU richness and estimated OTU richness based on the ACE nonparametric richness estimator shows three assemblages: top, middle, and bottom, with OTU richness increasing with depth (Fig. 3a). However, the Chao1 nonparametric richness estimator shows only the bottommost section to be significantly higher in OTU richness than the rest of the core. For most of the core, the average number of OTUs in the ice was slightly lower than that of the underlying seawater; however, the bottom section of the ice had a higher number of observed OTUs than that of the seawater (Fig. 3a). The melt pond assemblage shared *c.* 55% of its observed OTUs with the old ice assemblage and *c.* 28% of its observed OTUs with the new ice assemblage (Fig. S4). The old ice assemblage shared *c.* 35% of its observed richness with the new ice assemblage. The new ice assemblage showed the highest proportion of endemism, with over 75% unique OTUs; the assemblages of the old ice and melt pond layers had *c.* 60% and *c.* 41% unique OTUs, respectively (Fig. S4).

Overall diversity, which accounts for both OTU richness and OTU evenness, was estimated using two commonly utilized nonparametric diversity indexes: the Shannon diversity index (H') and inverse Simpson's index (1/D) (Fig. 3b). Both indexes showed that diversity increases with depth in the ice core, with a clear

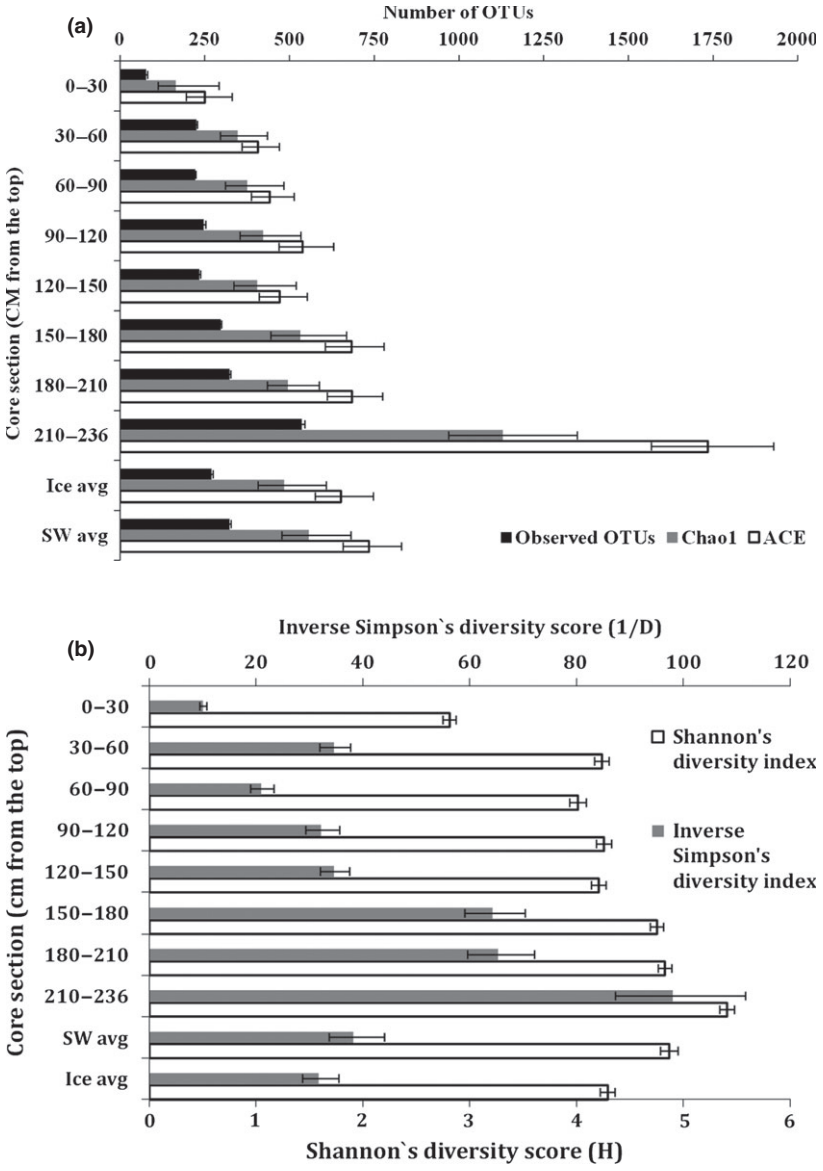

Fig. 3. Richness and diversity measurements along the core. (a) Observed and estimated (Chao1, ACE) OTU richness, (b) inverse Simpson's & Shannon's diversity indices for each sample. OTU definition set at 97% similarity.

separation of the values corresponding to the melt pond, old ice, and new ice layers.

There was no significant difference between the mean diversity of ice microbial assemblages and the mean diversity of water microbial assemblages.

Discussion

The analyzed core had three distinct assemblages: top (0 to 30 cm), middle (30 to 150 cm), and bottom (150 to 236 cm). Based on the bulk salinity profile and crystal texture of the core, the uppermost section was clearly a melt pond. The texture of ice crystals in the core and pore structure indicated that there was a break point at *c.* 125 cm depth, marking a separation between the 2-year-old ice and the *c.* 110 cm of new ice below that was added during the winter. The ice layering therefore matches well with our observed three layers in the microbial assemblage: the first layer (0 to 30 cm) is the melt pond assemblage; the second layer is the old ice assemblage (30 to 150 cm); and the third layer is the new ice assemblage (150 to 236 cm). The microbial assemblages of all three ice layers, including the permeable bottom layer, are quite distinct from the seawater microbial assemblage (Fig. 2), indicating a strong selection process during the formation and maturation of sea ice. Most likely, the sea ice assemblages are not homogenized with the seawater assemblages because the bacteria are attached to the ice surface within the ice structure (Mock & Thomas, 2005).

Texture analysis indicates that the ice from 120 to 150 cm contains both new and old ice; however, its assemblage composition clusters solely with the old ice. It is possible that as a new ice layer is formed, the temperature near the freezing front is still warm enough to allow mixing of seawater with the brines; therefore, it is likely that the established assemblage of the old ice influenced the composition of the new ice assemblage. That influence diminishes as the freezing front advances further down, away from the old ice, leading to the development of a distinct microbial assemblage. Another possible explanation is that DNA corresponding to members of the old ice assemblage was more easily extracted or PCR-amplified. Samples with higher resolution of sectioning, especially near the annual growth mark, are needed to differentiate between these explanations.

If the *in situ* physical and chemical gradients play a major role in structuring these bacterial assemblages, we would expect strong clustering of samples within ice sections. While the bacterial assemblages form distinct clusters related to depth within each layer, this clustering is not statistically significant. Thus, adaptation to environmental gradients was weak at best. The statistical uniformity in the structure of the old ice microbial assemblages may result from homogenization due to melt water and gravity-driven flushing of the ice and increased permeability during the summer. The new ice, on the other hand, is likely homogenized because it is permeable and therefore exchanges microorganisms freely between the sections and with the underlying seawater. Therefore, it appears that the water source of the ice is the driver of the assemblage structure and that the gradient in abiotic conditions plays a less significant role.

There is a top-to-bottom increase in both observed taxon richness and diversity, with a clear separation of the values corresponding to the melt pond, old ice, and new ice layers (Fig. 3). While the cause of the increased taxon richness and diversity with depth is unknown, it may be due to a decrease in how 'extreme' the environment is in depth, due to changes in *in situ* conditions such as ice permeability, temperature, salinity, and light levels. Therefore, while it appears that the *in situ* physical and chemical gradients may play a less significant role in structuring the composition of the MYI bacterial community, such gradients may be significant in affecting overall diversity.

Although comparing our work to others was not a main objective of this paper, we still nonetheless found some striking similarities to other studies of sea ice bacterial communities. Several past studies have quantified the taxon richness and diversity of bacterial assemblages from sea ice (Bowman *et al.*, 1997, 2011; Brown & Bowman, 2001; Petri & Imhoff, 2001; Junge *et al.*, 2002; Brinkmeyer *et al.*, 2003). While it is problematic to compare richness estimators as they tend to inflate with increased sequencing depth, the Shannon and Simpson diversity indexes tend to stabilize at a relatively low sequencing depth and thus are more suitable for such a comparison (Gihring *et al.*, 2012). Our mean Shannon diversity index values were similar to those of Bowman *et al.* (2012), who also analyzed a MYI sample using high throughput sequencing of 16S rRNA genes; however, both values were approximately threefold higher than for studies that did not use high throughput sequencing. Thus, higher sequencing depth shows significantly higher diversity in the sea ice, but at similar sequencing depths, MYI from different sites has similar levels of diversity.

The composition of bacterial assemblages in our sample was similar to that observed in other studies of sea ice bacterial assemblages (Bowman *et al.*, 1997, 2011; Petri & Imhoff, 2001; Junge *et al.*, 2002; Brinkmeyer *et al.*, 2003). *Alphaproteobacteria*, *Gammaproteobacteria*, *Bacteroidetes*, and *Verrucomicrobia* were prevalent components of the ice core in this study. However, unlike in some other sea ice samples, we found that *Actinobacteria* and *Betaproteobacteria* were prevalent in our samples, and we did not

find sequences related to the clade Chlamydiales. Thus, taxon richness, overall diversity, and community composition were similar between our sample and other sea ice samples, possibly indicating similar sea ice microbial communities in MYI globally.

Our results show a clear separation of the MYI bacterial assemblage to three groups corresponding to the three ice layers, both in composition and in diversity. There has been a decrease of *c.* 40% in the extent of MYI cover over the past three decades, with older, thicker ice cover lost more rapidly (Maslanik *et al.*, 2011), and it is likely that the Arctic Ocean will be MYI-free by the end of the century (Boé *et al.*, 2009). Refrozen melt pond ice and old ice will be absent from an FYI-covered Arctic Ocean. Although all three layers share many of the most abundant OTUs (Figs S3 and S4), our data suggests that about one-third of the observed taxa of the MYI core we sampled is found exclusively in the melt pond and old ice layers and therefore will be lost in an MYI-free Arctic Ocean. Due to the high degree of functional redundancy of bacterial communities, it is unclear what effect losing these unique bacterial taxa will have on the ecological functioning of sea ice bacterial communities. However, even if these unique taxa do not perform unique ecological functions, loss of biodiversity, and as consequence, functional redundancy reduces the resilience of an ecosystem and its ability to rebound from disturbance (Yachi & Loreau, 1999). As the Arctic Ocean shifts toward being MYI-free, calls of exploiting its vast resources are being voiced in the media frequently (Dodds, 2010). This will expose an ecosystem, already in limbo, to a potential multitude of anthropogenic disturbances. Therefore, further research is needed to understand the ecological functioning of the communities from each layer as well as those coming from newly formed ice sheets to understand its importance to the ecosystem.

Conclusions

Sea ice is a complex environment. Our study had a very modest sampling scheme, as we only sampled one site of landfast MYI; however, taxon richness, overall diversity, and assemblage composition all were similar to previous sea ice studies, indicating broad applicability of our findings. It is clear that the bacterial assemblage that colonizes MYI differs between each layer of ice (i.e. melt pond, old ice, new ice). These differences in the structure could imply differences in function of the assemblages in each of the layers. Furthermore, with the depletion of MYI, the Arctic will lose the old and melt pond ice layers and their associated bacterial assemblages. The loss of these layers, which have unique bacterial taxa, could impact the ecological functioning of the sea ice bacterial assemblage and potentially the Arctic Ocean as a whole in unknown ways.

Acknowledgements

B.D.L. and C.H. were supported by the Natural Science and Engineering Research Council of Canada (NSERC) Discovery Grant program and the Polar Continental Shelf Program (PCSP). C.H. was an Alberta Innovates – Technology Futures Fellow. I.H., B.L. and J.B. were supported by the Northern Scientific Training Program (NSTP) and Circumpolar-Boreal Arctic Research (C-BAR) programs. We would like to thank and acknowledge the PCSP support staff and CFS Alert for their support while in the field.

References

Boé J, Hall A & Qu X (2009) September sea-ice cover in the Arctic Ocean projected to vanish by 2100. *Nat Geosci* **2**: 341–343.

Bowman JP, McCammon SA, Brown MV, Nichols DS & McMeekin TA (1997) Diversity and association of psychrophilic bacteria in Antarctic sea ice. *Appl Environ Microbiol* **63**: 3068–3078.

Bowman JS, Rasmussen S, Blom N, Deming JW, Rysgaard S & Sicheritz-Ponten T (2012) Microbial community structure of Arctic multiyear sea ice and surface seawater by 454 sequencing of the 16S RNA gene. *ISME J* **6**: 11–20.

Brinkmeyer R, Knittel K, Jürgens J, Weyland H, Amann R & Helmke E (2003) Diversity and structure of bacterial communities in Arctic versus Antarctic Pack Ice. *Appl Environ Microbiol* **69**: 6610–6619.

Brown MV & Bowman JP (2001) A molecular phylogenetic survey of sea-ice microbial communities (SIMCO). *FEMS Microbiol Ecol* **35**: 267–275.

Comiso J (2010) Satellite remote sensing techniques. *Polar Oceans from Space* (Mysak L & Hamilton K, eds), pp. 73–111. Springer, New York.

Chao A (1984) Nonparametric estimation of the number of classes in a population. *Scand J Stat* **11**: 265–270.

Chao A & Shen T (2003) Nonparametric estimation of Shannon's index of diversity when there are unseen species in sample. *Environ Ecol Stat* **10**: 429–443.

Collins RE, Rocap G & Deming JW (2010) Persistence of bacterial and archaeal communities in sea ice through an Arctic winter. *Environ Microbiol* **12**: 1828–1841.

Cox GFN & Weeks WF (1983) Equations for determining the gas and brine volumes in sea-ice samples. *J Glaciol* **29**: 306–316.

Deming JW (2007) Life in ice formations at very cold temperatures. *Physiology and Biochemistry of Extremophiles*, (Gerday C & Glansdorf N, eds), pp. 133–145. ASM Press, Washington, DC.

Deming JW (2010) Sea ice bacteria and viruses. *Sea Ice*, 2nd. (Thomas DN & Dieckmann GS, eds), Wiley-Blackwell, Ames, IA.

Dodds K (2010) A polar Mediterranean? Accessibility, resources and sovereignty in the Arctic Ocean. *Global Policy* **1**: 303–311.

Dowd S, Sun Y, Secor P, Rhoads D, Wolcott B, James G & Wolcott R (2008) Survey of bacterial diversity in chronic wounds using Pyrosequencing, DGGE, and full ribosome shotgun sequencing. *BMC Microbiol* **8**: 43.

Edgar RC, Haas BJ, Clemente JC, Quince C & Knight R (2011) UCHIME improves sensitivity and speed of chimera detection. *Bioinformatics* **27**: 2194–2200.

Eicken H (2008) From the microscopic, to the macroscopic, to the regional scale: growth, microstructure and properties of sea ice. *Sea Ice: An Introduction to its Physics, Chemistry, Biology and Geology* (Thomas DN & Dieckmann GS, eds), pp. 22–81. Blackwell Science Ltd, Ames, IA.

Eicken H, Lensu M, Leppäranta M, Tucker WB III, Gow AJ & Salmela O (1995) Thickness, structure, and properties of level summer multiyear ice in the Eurasian sector of the Arctic Ocean. *J Geophys Res* **100**: 22697–22710.

Evans J, Sheneman L & Foster J (2006) Relaxed neighbor joining: a fast distance-based phylogenetic tree construction method. *J Mol Evol* **62**: 785–792.

Ewert M, Carpenter SD, Colangelo-Lillis J & Deming JW (2013) Bacterial and extracellular polysaccharide content of brine-wetted snow over Arctic winter first-year sea ice. *J Geophys Res* **118**: 726–735.

Gihring TM, Green SJ & Schadt CW (2012) Massively parallel rRNA gene sequencing exacerbates the potential for biased community diversity comparisons due to variable library sizes. *Environ Microbiol* **14**: 285–290.

Golden KM, Ackley SF & Lytle VI (1998) The percolation phase transition in sea ice. *Science* **282**: 2238–2241.

Gosselin M, Levasseur M, Wheeler PA, Horner RA & Booth BC (1997) New measurements of phytoplankton and ice algal production in the Arctic Ocean. *Deep Sea Res Part II–Topical Stud Oceanogr* **44**: 1623–1644.

Haas C (2004) Late-summer sea ice thickness variability in the Arctic Transpolar Drift 1991–2001 derived from ground-based electromagnetic sounding. *Geophys Res Lett* **31**: L09402.

Harding T, Jungblut AD, Lovejoy C & Vincent WF (2011) Microbes in high Arctic snow and implications for the cold biosphere. *Appl Environ Microbiol* **77**: 3234–3243.

Helmke E & Weyland H (1995) Bacteria in sea ice and underlying water of the eastern Weddel sea in midwinter. *Mar Ecol Prog* **117**: 269–287.

Hobbie JE, Daley RJ & Jasper S (1977) Use of Nucleopore filters for counting bacteria by fluorescence microscopy. *Appl Environ Microbiol* **33**: 1225–1228.

Huse SM, Welch DM, Morrison HG & Sogin ML (2010) Ironing out the wrinkles in the rare biosphere through improved OTU clustering. *Environ Microbiol* **12**: 1889–1898.

Jungblut AD, Lovejoy C & Vincent WF (2009) Global distribution of cyanobacterial ecotypes in the cold biosphere. *ISME J* **4**: 191–202.

Junge K, Krembs C, Deming J, Stierler A & Eicken H (2001) A microscopic approach to investigate bacteria under in situ conditions in sea-ice samples. *Annal Glaciol* **33**: 304–310.

Junge K, Imhoff F, Staley T & Deming JW (2002) Phylogenetic diversity of numerically important Arctic sea-ice bacteria cultured at subzero temperature. *Microb Ecol* **43**: 315–328.

Junge K, Eicken H & Deming JW (2004) Bacterial activity at −2 to −20°C in Arctic wintertime sea ice. *Appl Environ Microbiol* **70**: 550–557.

Junge K, Eicken H, Swanson BD & Deming JW (2006) Bacterial incorporation of leucine into protein down to -20 degrees C with evidence for potential activity in sub-eutectic saline ice formations. *Cryobiology* **52**: 417–429.

Kaartokallio H, Laamanen M & Sivonen K (2005) Responses of Baltic Sea ice and open-water natural bacterial communities to salinity change. *Appl Environ Microbiol* **71**: 4364–4371.

Kaartokallio H, Tuomainen J, Kuosa H, Kuparinen J, Martikainen PJ & Servomaa K (2008) Succession of natural sea-ice bacterial communities in the Baltic Sea fast ice. *Polar Biol* **31**: 783–793.

King MD, France JL, Fisher FN & Beine HJ (2005) Measurement and modelling of UV radiation penetration and photolysis rates of nitrate and hydrogen peroxide in Antarctic sea ice: an estimate of the production rate of hydroxyl radicals in first-year sea ice. *J Photochem Photobiol, A* **176**: 39–49.

Lozupone C, Hamady M & Knight R (2006) UniFrac – An online tool for comparing microbial community diversity in a phylogenetic context. *BMC Bioinformatics* **7**: 371.

Maslanik J, Stroeve J, Fowler C & Emery W (2011) Distribution and trends in Arctic sea ice age through spring 2011. *Geophys Res Lett* **38**: L13502.

McMinn A & Hegseth E (2007) Sea ice primary productivity in the northern Barents Sea, spring 2004. *Polar Biol* **30**: 289–294.

McMinn A, Ryan K, Ralph P & Pankowski A (2007) Spring sea ice photosynthesis, primary productivity and biomass distribution in eastern Antarctica, 2002–2004. *Marine Biol* **151**: 985–995.

Mock T & Thomas DN (2005) Recent advances in sea-ice microbiology. *Environ Microbiol* **7**: 605–619.

Petri R & Imhoff J (2001) Genetic analysis of sea-ice bacterial communities of the Western Baltic Sea using an improved double gradient method. *Polar Biol* **24**: 252–257.

Poltermann M (2001) Arctic sea ice as feeding ground for amphipods – food sources and strategies. *Polar Biol* **24**: 89–96.

Porter KG & Feig YS (1980) The use of DAPI for identification and enumeration of bacteria and blue-green algae. *Limnol Oceanogr* **25**: 943–948.

Pruesse E, Quast C, Knittel K, Fuchs BM, Ludwig W, Peplies J & Glöckner FO (2007) SILVA: a comprehensive online resource for quality checked and aligned ribosomal RNA sequence data compatible with ARB. *Nucleic Acids Res* **35**: 7188–7196.

Quince C, Lanzen A, Curtis TP, Davenport RJ, Hall N, Head IM, Read LF & Sloan WT (2009) Accurate determination of microbial diversity from 454 pyrosequencing data. *Nat Methods* **6**: 639–641.

Quince C, Lanzen A, Davenport RJ & Turnbaugh PJ (2011) Removing noise from pyrosequenced amplicons. *BMC Bioinformatics* **12**: 38.

Riedel A, Michel C, Gosselin M & LeBlanc B (2008) Winter-spring dynamics in sea-ice carbon cycling in the coastal Arctic Ocean. *J Mar Syst* **74**: 918–932.

Schloss PD (2010) The effects of alignment quality, distance calculation method, sequence filtering, and region on the analysis of 16S rRNA gene-based studies. *PLoS Computational Biol* **6**: e1000844.

Schloss PD, Westcott SL, Ryabin T *et al.* (2009) Introducing mothur: open-source, platform-independent, community-supported software for describing and comparing microbial communities. *Appl Environ Microbiol* **75**: 7537–7541.

Schloss PD, Gevers D & Westcott SL (2011) Reducing the effects of PCR amplification and sequencing artifacts on 16S rRNA-based studies. *PLoS ONE* **6**: e27310.

Shannon CE (1948) A mathematical theory of communication. *Bell Syst Tech J* **27**: 379–423.

Simpson EH (1949) Measurement of diversity. *Nature* **163**: 688.

Wadhams P (2000) *Ice in the Ocean*. Gordon and Breach Science Publishers, London, UK.

Wing S, McLeod R, Leichter J, Frew R & Lamare M (2012) Sea ice microbial production supports Ross Sea benthic communities: influence of a small but stable subsidy. *Ecology* **93**: 314–323.

Yachi S & Loreau M (1999) Biodiversity and ecosystem productivity in a fluctuating environment: the insurance hypothesis. *Proc Natl Acad Sci USA* **96**: 1463–1468.

Yue JC & Clayton MK (2005) A similarity measure based on species proportions. *Comm Stat–Theory and Methods* **34**: 2123–2131.

Supporting Information

Additional Supporting Information may be found in the online version of this article:

Fig. S1. Cell concentrations and temperature profile.
Fig. S2. Rarefaction and rank abundance curves.
Fig. S3. Heat map of OTU distribution through sea ice.
Fig. S4. Venn diagram of shared OTUs in sea ice.
Table S1. Oligonucleotide sequences used in this manuscript.
Table S2. Dominant OTUs (> 10%) for each dominant class per ice layer including averaged relative proportions per layer within the phylum.
Table S3. Dominant OTUs (> 10%) for each dominant phylum per ice group including relative proportions within the phylum.